IEEE Photonics Journal
An IEEE Photonics Society Publication

Open Access

Simulations of Pump Absorption in Tandem-Pumped Octagon Double-Clad Fibers

Volume 13, Number 2, April 2021

Martin Grábner, *Member, IEEE*
Kanagaraj Nithyanandan
Pavel Peterka
Pavel Koška
Ali. A. Jasim
Pavel Honzátko

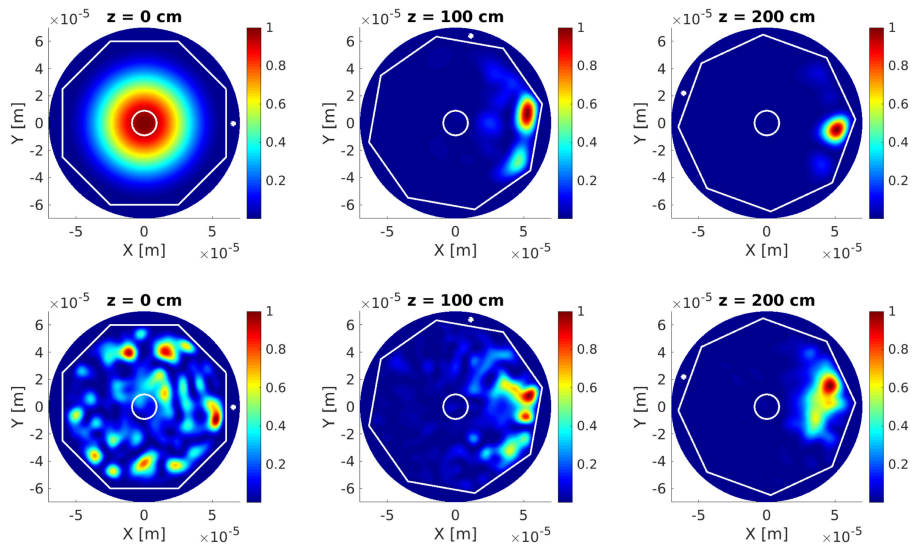

DOI: 10.1109/JPHOT.2021.3060857

Simulations of Pump Absorption in Tandem-Pumped Octagon Double-Clad Fibers

Martin Grábner,[1] ***Member, IEEE***, **Kanagaraj Nithyanandan**,[2,3] **Pavel Peterka**,[1] **Pavel Koška**,[1] **Ali. A. Jasim**,[1] **and Pavel Honzátko**[1]

[1]Institute of Photonics and Electronics, Czech Academy of Sciences, Chaberská 1014/57 Praha 8, Praha 182 51, Czech Republic
[2]Department of Physics, Indian Institute of Technology Hyderabad, Kandi, Telangana 502285, India
[3]Optoelectronic Research Centre, University of Southampton, Southamtpon SO17 1BJ, U.K.

DOI:10.1109/JPHOT.2021.3060857

Manuscript received December 9, 2020; accepted February 16, 2021. Date of publication February 22, 2021; date of current version March 18, 2021. This work was supported by Czech Science Foundation through the Project 19-03141S. Corresponding author: Martin Grábner (e-mail: grabner@ufe.cz).

Abstract: The cladding pumping within a double-clad fiber structure is an effective technique to convert high-power multimode beam into high-power, almost diffraction limited beam. Since the pump efficiency is limited by the presence of higher skew-ray modes, geometrical perturbations are used to scramble the modes and to achieve a higher overlap of the electromagnetic field with the doped core. In this paper, the combined effect of fiber coiling and twisting is investigated in the double-clad fiber structure with the octagonal shape of an inner cladding. Electromagnetic field propagation through fibers with different cross-section areas, bending radii and twisting rates is numerically simulated using finite element beam propagation method. Holmium-doped double-clad fiber pumped in tandem configuration at wavelength 1950 nm is selected as an example. Nontrivial dependence of pump absorption on bending radius with the presence of local maxima is revealed. The observed impact of fiber coiling and twisting increases with the size of the cross-section area of the inner cladding.

Index Terms: Double-clad fiber, finite element beam propagation, pump absorption, fiber laser.

1. Introduction

High power fiber lasers are the subject of intense research owning to their potential applications in different areas of industry, research, medicine, security and others [1]. The high power scaling of fiber lasers was enabled by the invention of optical pumping through large inner cladding of the so-called double-clad (DC) fiber structures, see Fig. 1(a). Of late, the emphasis is particularly given to improve the performance, efficiency and power scaling capabilities of novel DC fibers. Large area and high numerical aperture of inner cladding waveguide allow for efficient coupling of low quality high power beam of standard multimode laser diodes. The pump is absorbed in a rare-earth-doped core that finally emits high-quality, preferably single-transverse mode laser output, see Fig. 1(b). In such a way, DC fibers act as highly efficient transformers of low-quality beams of high-power laser diodes into high-quality, almost diffraction-limited laser beams. Fiber lasers with kilowatt range

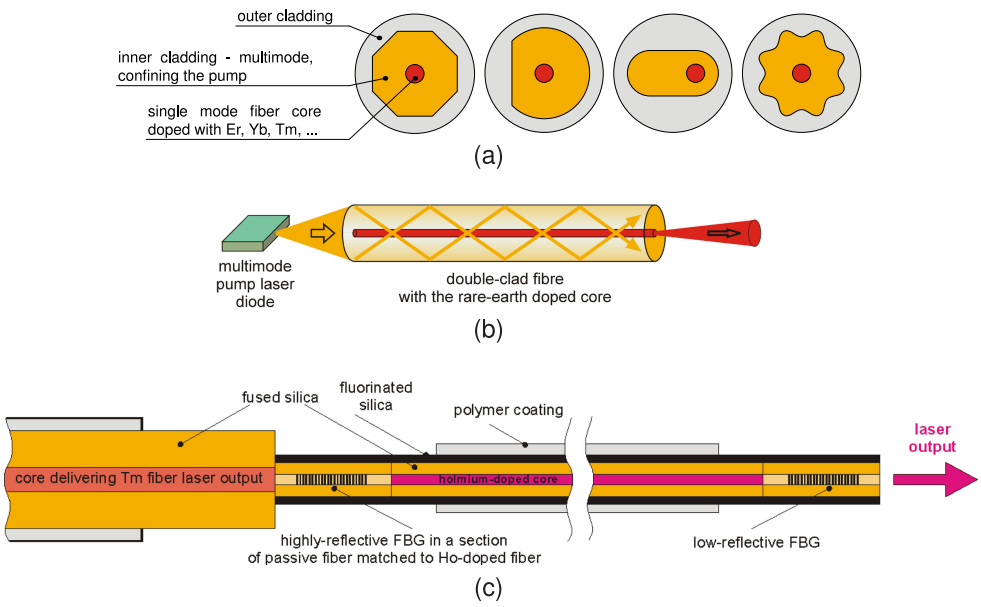

Fig. 1. The principle of the cladding pumping of the DC active fiber: (a) Cross-section of the DC active fiber with the inner cladding shapes: octagonal, D-shaped, stadium and flower [16]. (b) Laser diode pumping schematic: transformation of the high-power, low-quality pump beam from laser diode into high-power high quality, almost diffraction limited laser signal. Note that laser diode light coupling is shown only schematically. Usually, laser diode light is firstly coupled into a pump delivery fiber. (c) Tandem pumping schematic: an example of all-fiber configuration tandem pumping of holmium fiber laser with a fiber Bragg grating (FBG).

output powers typically up to about 5 kW [2]–[4] can be built using direct pumping by laser diodes. The output powers of 10 kW were recently demonstrated using advanced fiber designs and diode pumping [5], [6]. To reach even higher laser power emission from a single rare-earth-fiber, i.e., without a combination of multiple fiber laser outputs, another pumping scheme has to be used so that the thermal load of the final DC fiber amplifier is reduced. Up to 20 kW of output power at around 1070 nm from the single double-clad fiber was demonstrated by the so-called tandem pumping configuration, where high brightness, in-band optical pumps at slightly shorter wavelength of 1018 nm were combined into a single DC fiber [7], [8]. Courtesy of high-brightness pumps, typically other fiber lasers, one can design smaller inner cladding size of the DC fibers used in tandem pumping setups.

Tandem pumping scheme is particularly important for efficient power scaling of fiber lasers with larger quantum defect when directly pumped by multimode pump laser diodes. Namely it is the case of thulium fiber lasers, e. g., emitting at around 2 μm and pumped by other thulium fiber lasers at slightly lower wavelengths [9], and in holmium fiber lasers at 2.1 μm pumped by thulium fiber lasers at around 1.95 μm [10], [11], see example of all-fiber tandem pumped setup in Fig. 1(c). Holmium-doped silica-based fiber lasers are of increasing importance especially for remote atmospheric monitoring thanks to extended operation range in atmospheric window 2025-2250 nm [12], [13] and for nonlinear frequency conversion in zinc-germanium-phosphide crystals and for defense applications [14], [15]. It should be noted that fiber lasers pumped at around 1.9-2 μm also require outer claddings made out of glass because polymer outer claddings exhibit relatively large absorption at this wavelength range which causes thermal damage to polymer coatings.

Efficient coupling of the pump power into the active region of the DC fiber is the key condition to achieve a high power output of fiber lasers. The performance of DC fibers with a circular inner cladding is known to be impaired by the presence of higher skew-ray modes. These modes exhibit a low overlap with a doped absorbing core and thus propagate along with the fiber without significant absorption. To remedy this effect and to increase the efficiency of energy transfer into a core the

modes are deliberately scrambled utilizing fiber geometry perturbation in its cross-section shape and also by applying longitudinal deformations such as bent and twist. For example the D-shape, regular polygon or stadium belong among the cross-section inner cladding shapes that have been investigated both experimentally and theoretically [1]. Moreover, with the advanced technology of shaping optical fiber preforms with a CO_2 laser it is possible to fabricate even more complex shapes with non-flat edges such as a flower shape, see Fig. 1(a). Such complex shapes with a concave and convex form showed to have a positive impact on enhancing the pump absorption [17], [18]. Unconventional fiber bending and coiling layouts that have been studied are for example the figure of eight [19], [20], kidney-shaped [21], stadium [22], spiral [23] or tight coiling on the standard circular shape of spool [24]. The experimental investigation of pump absorption in the Tm-doped octagonal DC fiber with 120 μm flat-to-flat dimension was presented in [25] where the effect of coiling and twisting was demonstrated even for the case of almost straight fiber layout. The choice of a particular combination of fiber deformations is expected to influence the pump absorption and thus the energy transfer to the laser output. Nevertheless, the problem of pump absorption optimization is a multi parameter global optimization problem involving a large number of variables and therefore it is hard to solve without numerical modeling.

Methodology for rigorous numerical modelling was reported that allows for description of the effect of bending and twisting of the DC fibers on the pump absorption in DC fiber structures [26]–[28]. This methodology opened a new way to design double-clad fibers for optimized or tailored pump absorption. Very broad range of fiber designs is worth to study and non-intuitive conclusions, important for fiber laser technology, can be deduced using this methodology. However, highly demanding computation is probably the reason why such methodology was so far used only by several laboratories worldwide and for limited practical case studies [23]–[25], [27]–[29]. Numerical simulations have shown the effect of bending and twisting of the DC fibers of hexagonal and stadium cross-sections [27]–[31] In these works, not only the effect of mode scrambling was demonstrated but also the effects of squeezing and decentering of the optical pump transversal distribution. Several regular polygonal structures and bending layouts were also studied without twisting [22], [23].

Despite these efforts, the task of finding optimum geometrical settings that lead to maximizing the pump absorption is far from being complete as there still remains a lack of understanding of the interplay of geometrical parameters of the problem such as the bending radius and the twist rate. Furthermore, there is an influence of the excitation field launched to the fiber since its modal structure has to be considered for a comprehensive picture. Fiber designs for tandem pumping that are often characterized by a relatively small inner cladding of the DC fiber are the particular examples of structures that have not been analyzed thoroughly so far.

In this paper, we study, by means of numerical simulations, a particular problem of pump propagation in the DC fibers with widely used octagonal cladding to quantify the effect of the bending radius and the twist rate for several cross-section geometries and excitation electromagnetic fields of the pump. As an example, the holmium-doped core DC fiber is considered in simulation with a pumping wavelength 1950 nm, typically in tandem pumping configuration according to Fig. 1(c). This choice is motivated by recent advances in holmium doped fibers [14], [15], [13], [10] and interest in their modeling [32] but it should be noted that the conclusions are applicable also to another types of rare-earth doped fibers intended especially for tandem-pumped configuration.

The paper is organized as follows. Following the introduction, Section 2 brings out the overview of the numerical model. The selected simulation results for the representative fiber geometries are presented in Section 3. Section 4 discuss the results of the simulations and Section 5 concludes the paper with summary of results.

2. Numerical Model

Numerical modeling is done using the finite element beam propagation method (FEM-BPM) and follows the approach presented in [27], [28], [29]. FEM-BPM uses 3 components of electric field in its algorithm and thus it is a full-vectorial method with conventional unidirectional beam propagation.

TABLE 1
Octagon Double Cladding Fiber Parameters for Five Simulated Geometries

Geometry size abbreviation (FtF/$2a$)		G-1 (30/10)	G-2 (30/5)	G-3 (65/14)	G-4 (65/5)	G-5 (120/18)
Cladding flat-to-flat dimension, FtF	µm	30	30	65	65	120
Core diameter, $2a$	µm	10	5	14	5	18
Num. aperture of core, NA_c	-	0.12	0.24	0.12	0.24	0.08
Num. aperture of cladding, NA_1	-	0.22	0.22	0.22	0.22	0.22
Core absorption, α	m^{-1}	21.88	87.48	52.38	410.83	107.99
Ho^{3+} concentration	mol ppm	3584	14330	8580	67300	17690
Ho^{3+} concentration, N	$10^{25}m^{-3}$	7.54	30.2	18.1	142	37.2
Ho^{3+} mass fraction, wt	%	0.93	3.68	2.22	15.85	4.51
$Im(n_c)$	10^{-6}	-3.395	-13.574	-8.127	-63.751	-16.756
Octagon area, S_{clad}	μm^2	746	746	3500	3500	11929
Ideal clad. pump absorption, A_{ideal}	dB/m	10.0	10.0	10.0	10.0	10.0
Pump delivery fiber core diameter	µm	28	28	63	63	118

Five octagonal cross-sectional geometries were chosen for propagation simulations with flat-to-flat (FtF) size of 30 μm, 65 μm [13] and 120 μm [14], [10] and different core radii. The parameters of the fibers with different geometries are summarized in Table 1. The refractive index of the inner cladding is $n_1 = 1.4388$ which is the refractive index of SiO_2 at wavelength $\lambda = 1.95$ μm. The refractive indices of the core n_c and of the outer cladding n_2 are obtained from the numerical aperture of the core NA_c and of the inner cladding NA_1 as $n_c^2 = n_1^2 + NA_c^2$, $n_2^2 = n_1^2 - NA_1^2$. The absorption in the core is modeled by the imaginary part of refractive index:

$$Im(n_c) = -\alpha \frac{\lambda}{4\pi} \tag{1}$$

where α [m^{-1}] is core absorption and λ [m] is wavelength. The equation (1) comes from the fact that in an absorbing medium with the complex refractive index n_c the field changes with distance z as $E(z) = E_0 \exp(-ik_0 n_c z)$ where $k_0 = 2\pi/\lambda$ is a wavenumber and power is $P(z) \propto |E(z)|^2$. The core is doped with Ho^{3+} ions with concentration N [m^{-3}] such that the material absorption of the core is:

$$\alpha = N\sigma_a \tag{2}$$

where $\sigma_a = 2.90 \cdot 10^{-25}$ m ^{2} is the absorption cross-section of Ho^{3+} for pump wavelength $\lambda = 1.95$ μm. Note that since the focus is on the pump absorption of the fibers with specific cross sections and layouts, saturation of absorption through the full set of laser rate equations is not included in the numerical model. The values of the concentration N applied in simulations are chosen to achieve a fixed value of the ideal cladding pump absorption $A_{ideal} = 10$ dB/m. This is attributed to work with single ideal cladding pump absorption and to facilitate comparison with the other geometries of interest for better quantitative understanding. The ideal absorption scales with the ratio of core area S_{core} and core plus inner cladding area S_{clad} as

$$A_{ideal} = 4.34\alpha(S_{core}/S_{clad}). \tag{3}$$

The DC fiber cross-section structure is shown in Fig. 2(a). It is discretized by a triangular mesh with maximal element size h in the core and inner cladding equal to $h = \lambda/2$. Fig. 2(b) shows the generated 2D mesh [33] for the geometry G-1 (30/10). The longitudinal propagation step is $dz = 10$ μm. The element size and step values were chosen to guarantee the numerical stability and sufficient accuracy.

Fiber bending with a bending radius R is modeled (for bending in x-direction) by an inhomogeneous but isotropic refractive index profile $n_b(x, y) = n(x, y)(1 + x/R)$ that is based on conformal transformation [34]; $n(x, y)$ is the original physical refractive index profile of the fiber cross-section.

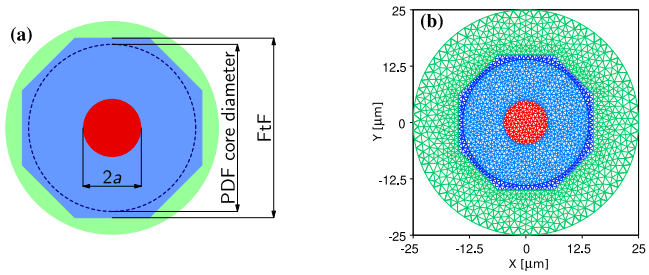

Fig. 2. (a) DC fiber cross-section with octagonal shape of the inner cladding including pump delivery fiber (PDF) core area (dashed line). (b) 2D mesh of fiber cross-section for geometry G-1 (FtF $= 30$ μm).

The effect of simultaneous *bending and twisting* is approximated by the formula [27]:

$$n_{bt}(x, y) = n(x, y)\left(1 + \frac{[x, y] \cdot [\cos(\phi), \sin(\phi)]}{R}\right) \tag{4}$$

where ϕ is the twist angle given by $\phi = (\pi/180)tr \cdot z$ where z [m] is longitudinal coordinate (that is increasing during FEM-BMP simulation) and tr [deg/m] is a twisting rate. Anisotropy due to material stress in the twisted fiber is neglected. The refractive index profile is updated by (4) at discrete longitudinal distances with a 1 mm step. In post-processing, the transversal coordinates x, y of the mesh nodal points are interpreted as rotated in a clock-wise direction along the fiber. In the limit of the small twisting rate, the transverse field rotates together with a fiber cross-section shape which is in accordance with intuition of a field propagating in a slowly twisted waveguide. However, it should be noted that the accuracy of such approximation is reducing with increasing a twist rate. Furthermore, it has to be noted that the formula (4) does not introduce any twisting related perturbation in the limit of large bending radii $R \to \infty$ and thus the assesment of the twisting effect in nearly straight fibers is limited.

The values of maximum mesh element size h, longitudinal propagation step dz and twisting update step mentioned above were selected such that simulations provide sufficiently accurate results on one hand yet relatively low simulation times on the other hand. For example, the error in simulated absorption of about 0.2 dB/m was observed in the case of propagation of the fundamental mode of the octagon fiber with a strongly doped core having a nominal mode loss $A_{\text{mod}} \approx 98$ dB/m where the mode loss is derived from the imaginary part of the effective refractive index of the mode by a relation equivalent to (1).

Four types of initial field excitation localized within a pump delivery (PD) fiber core diameter (see Figs. 2(a) and 1(c)) are considered :

1) The fundamental mode of the PD fiber.
2) The flat top pattern of linearly polarized field over the diameter equal to a PD fiber core diameter, see Table 1.
3) Speckle field pattern.
4) Skew-ray mode pattern.

The speckle field is generated by propagating the fundamental mode of pump delivery fiber through 4 sections of 10 cm length where the first and third sections are bent with radius 3 cm along x and y axes. This way is chosen to be consistent with previous works [28]. The speckle field excitation is considered and applied only in the DC fiber with the largest cross-section area with FtF $= 120$ μm (geometry G-5). This is attributed to the fact that only the largest geometry supporting high enough modes can create the typical speckle field by a realistic perturbation of the fiber.

For a comprehensive picture on the role of the initial excitation, we also demonstrate the absorption in the event of skew-ray excitation which is generally proven to be poor in terms of the pump absorption. Skew-ray modes are chosen such that the mode overlap factor with a core, Γ, is sufficiently small or practically negligible, see Table 2. The overlap factor (or relative core

TABLE 2
The Skew-Ray Modes Selected for Given Geometry and Respective Mode Overlap Factors With the Core

Geometry	G-1	G-2	G-3	G-4	G-5
Mode	EH_{21}	EH_{22}	EH_{54}	EH_{54}	EH_{76}
Γ [dB]	-21.9	-32.7	-28.9	-86.6	-50.8

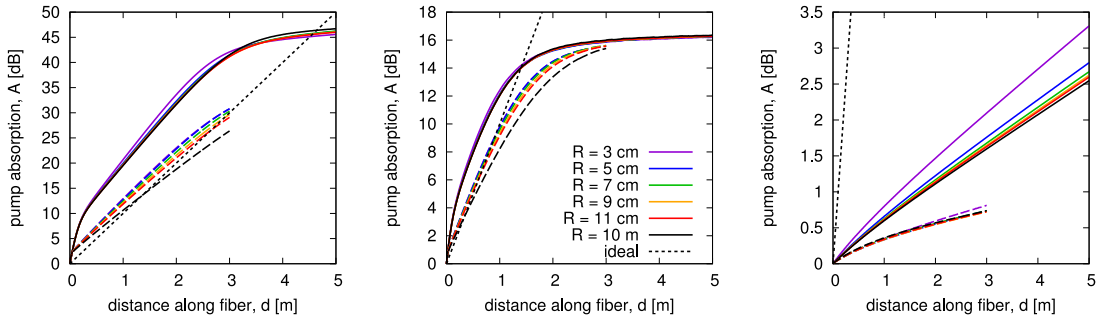

Fig. 3. Left: Pump absorption along the fiber excited by a PD fiber fundamental mode (excitation 1), solid lines for geometry G-1 (30/10), dashed lines for geometry G-2 (30/5). Center: Pump absorption along the fiber excited by a flat-top field (excitation 2), solid lines for geometry G-1 (30/10), dashed lines for geometry G-2 (30/5). Right: Pump absorption along the fiber excited by a skew-ray mode (excitation 4), solid lines for geometry G-1 (30/10), dashed lines for geometry G-2 (30/5). (FtF $= 30$ μm) Legend is the same for all plots.

power) for the case of a homogeneously doped core is defined as:

$$\Gamma = \int_{S_{\text{core}}} P_z \mathrm{d}S \Big/ \int_{S_{\text{clad}}} P_z \mathrm{d}S \tag{5}$$

where P_z is the z component of the Poynting vector. The skew-ray mode propagates outside the core and has to be scrambled to achieve any absorption in doped core. Thus the effect of mode scrambling becomes more evident when this kind of excitation is applied.

Bending radius R and twisting rate tr are the varied parameters during simulations. Using large value of bending radius $R = 10$ m approximates propagation in the straight fiber.

3. Simulation Results

The large amount of data was obtained from the numerical simulations of propagation in DC fibers with different geometries, excitation fields and layout perturbation parameters. In this section, the selected results are provided to demonstrate the main characteristics of pump absorption in DC fibers. The simulation results consist of 1) the pump absorption evolution along the fiber length, 2) the evolution of the fraction of power in the core along the fiber. These are presented separately for different geometries with the same flat-to-flat size in order to reveal the effect of core radius.

3.1 Geometry G-1 (30/10) and G-2 (30/5)

Fig. 3 (left) shows the pump absorption evolution along the DC fiber with FtF $= 30$ μm excited by a fundamental mode of PD fiber for geometries with different core radius. In geometry G-1 (30/10), the absorption increases initially much faster than expected from (3) (A_{ideal} is plotted by a dotted line in Fig. 3). This is the consequence of a large overlap of the PD fiber's fundamental mode with the doped core of the DC fiber and is also documented by a large value of relative core power at the beginning of the fiber, see Fig 4. The field is propagated up to 5 m distance for geometry

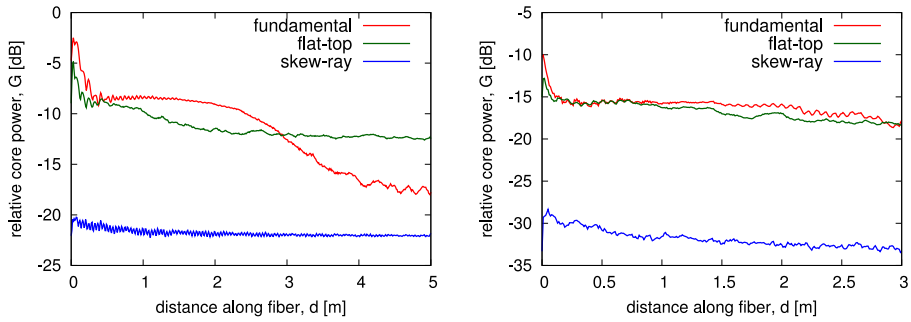

Fig. 4. Relative power in the core along the fiber, $R = 3$ cm, $tr = 1$ deg/mm. Left: geometry G-1 (30/10), right: geometry G-2 (30/5), (FtF $= 30$ μm).

G-1 (30/10) and pump absorption is saturated when $d > 3$ m. Note that the simulated fiber length 5 m used for geometry G-1 was chosen also to check the numerical stability of the computational algorithm. In simulations with other geometries, the field is propagated only up to 3 m distance since it is sufficient to determine all characteristics of our interest. Absorption in geometry G-2 (30/5) is smaller than in geometry G-1 due to smaller core.

Fig. 3 (center) shows the pump absorption evolution along the DC fiber excited by a flat-top pattern. Absorption value is saturated above 15 dB and is smaller than in previous excitation case because of smaller overlap of the flat-top field with the core. Absorption is clearly not dependent on bending radius R and twisting rate tr.

Fig. 3 (right) shows the pump absorption along the fiber excited by a EH_{21} mode (geometry G-1) and by a EH_{22} mode (geometry G-2) of the PD fiber respectively. The skew-ray modes EH_{21}, EH_{22} have a low overlap with the core of the DC fiber and they are about the highest bounded (skew-ray) modes supported by the PD fiber of a given size. The pump power is not much absorbed since the fiber perturbation cannot achieve an efficient mode mixing in the structures where only a low number of modes can propagate.

Fig. 4 shows the evolution of a relative core power (RCP), determined by (5), along the fiber for different excitation fields. The input RCP is large when the DC fiber is excited by the fundamental mode or the flat-top field. On the other hand, RCP remains low along the whole fiber in the case of skew-ray excitation having a low overlap with the core. The energy conversion from the skew-ray mode to the modes with a larger core overlap is small and consequently the resulting pump absorption is much smaller than the A_{ideal}.

The DC fibers with the smallest FtF considered so far exhibit generally low if any sensitivity of pump absorption to longitudinal perturbations. As the number of supported modes increases in a larger structure, one can anticipate greater sensitivity in geometries G-3 and G-4 studied in the next section.

3.2 Geometry G-3 (65/14) and G-4 (65/5)

We extend the investigation to geometries with relatively larger FtF $= 65$ μm. Fig. 5 (left) shows the pump absorption evolution along the DC fiber for geometries G-3 (65/14) and G-4 (65/5) excited by a fundamental mode of the PD fiber. It is apparent that the pump absorption increases with a bending radius R. The geometry G-4 with a smaller core exhibit lower absorption due to lower overlap of the initial field with the core. A very similar absorption dependence can be seen in Fig. 5 (center) for the DC fiber excited by a flat-top field.

Fig. 5 (right) shows the pump absorption evolution along the DC fiber excited by the skew-ray EH_{54} mode of the PD fiber. The values of achieved absorption are similar to flat-top case despite the fact that, as demonstrated in Fig. 6, the initial RCP is as small as -28 dB. However RCP

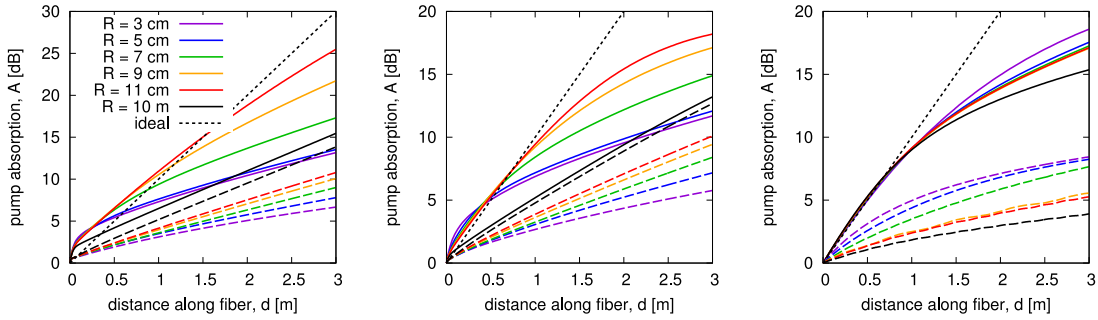

Fig. 5. Left: Pump absorption along the fiber excited by a PD fiber fundamental mode (excitation 1), solid lines for geometry G-3 (65/14), dashed lines for geometry G-4 (65/5). Center: Pump absorption along the fiber excited by a flat-top field (excitation 2), solid lines for geometry G-3 (65/14), dashed lines for geometry G-4 (65/5). Right: Pump absorption along the fiber excited by a skew-ray mode (excitation 4), solid lines for geometry G-3 (65/14), dashed lines for geometry G-4 (65/5). (FtF $= 65$ μm) Legend is the same for all plots.

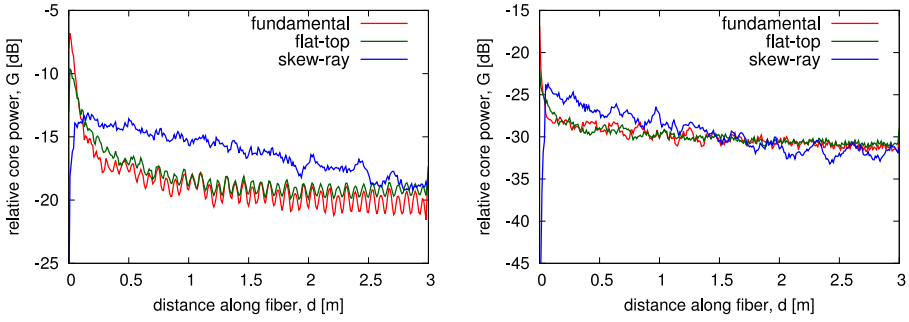

Fig. 6. Relative power in the core along the fiber, $R = 3$ cm, $tr = 1$ deg/mm. Left: geometry G-3 (65/14), right: geometry G-4 (65/5), (FtF $= 65$ μm).

raises fast up to -14 dB and then decreases slowly along the fiber. The mode mixing is more efficient in the geometry G-3 (65/14) comparing to the geometry G-1 (30/10) which results in a larger pump absorption that is up to distance 1 m well approximated by A_{ideal}. Similar behavior is observed in the geometry G-4 (65/5) with a smaller core resulting in smaller values of absorption. The pump absorption in the DC fibers with the larger FtF $= 65$ μm considered here has notable sensitivity to fiber bending. However as it will be presented in Section 4 fiber twisting does not provide much further improvement of absorption in these geometries. Based on some previous studies (e.g. [30]), one may suspect that this will change for field propagating in structures with even larger cross-section area supporting a higher number of propagation modes. The results of geometry G-5 that are presented in the next section seem to confirm such assumption.

3.3 Geometry G-5 (120/18)

Fig. 7 (left) shows the pump absorption along the fiber excited by a fundamental mode of the PD fiber and by a flat-top field. Still smaller absorption values, $A < 12$ dB (lower then straight fiber absorption), are achieved in comparison with smaller geometries with the same input fields. Again flat-top excitation gives slightly lower absorption then the fundamental mode. Speckle pattern field and skew-ray mode characteristics are shown in Fig. 7 (right). Interestingly, the highest absorption is achieved in the DC fiber fed by a skew-ray mode and bent with the bending radius $R = 3$ cm. In this case, the significant influence of fiber perturbation is evident as there is large difference in

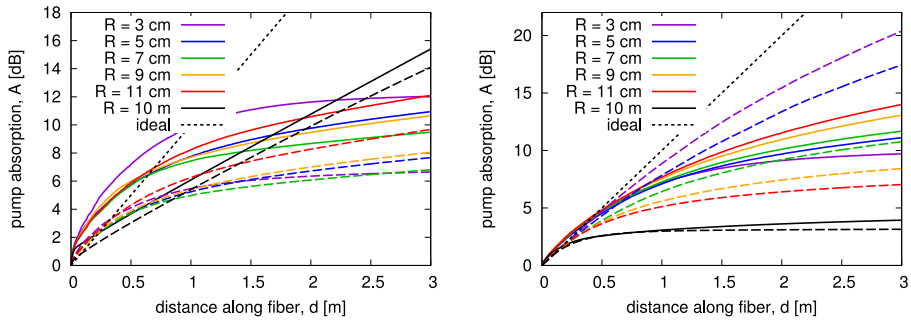

Fig. 7. Left: Pump absorption along the fiber, geometry G-5 (120/18). solid lines for PD fiber fundamental mode (excitation 1), dashed lines for flat-top field (excitation 2). Right: Pump absorption along the fiber, geometry G-5 (120/18). solid lines for speckle field (excitation 3), dashed lines for skew-ray mode (excitation 4).

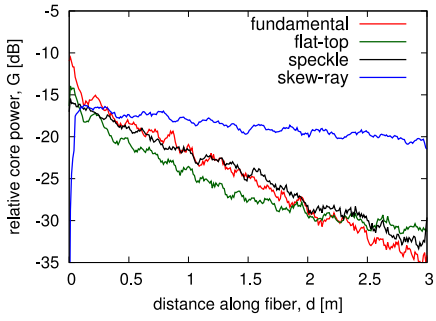

Fig. 8. Relative power in the core along the fiber, $R = 3$ cm, $tr = 1$ deg/mm, geometry G-5 (120/18), (FtF $= 120$ μm).

absorption in a straight fiber with $A < 4$ dB and in bent fiber with $R = 3$ cm giving $A > 20$ dB at the fiber end.

This behavior is further documented in Fig. 8 where RCP dependencies for different input fields are compared. RCP increases quickly from about -50 dB up to -16 dB and decreases with distance slowly for skew-ray excitation. In other three cases, RCP is reduced steadily and much faster with a distance.

To illustrate the field evolution along the fiber (distances $z = 0100$, 200, 300 cm) for geometry G-5 (FtF $= 120$ μm), we show in Fig. 9, the field distribution for different excitations. The fiber cross-section is rotated in a clockwise direction; the reference point is denoted by an asterisk. An output field is very similar for all excitation field cases except of the skew-ray mode EH_{76} excitation. In cases of excitations 1-3, the field is pushed to the right side that is the outer side of fiber bending. It was checked that the results similar to EH_{76} are also achieved by applying EH_{54} mode.

The largest geometry provides the results qualitatively similar to studies of the large hexagonal DC fiber structure that were made before, see Ref. [30]. However the examples presented in Section 3 constitute only a smaller part of the obtained numerical data. In order to see the full picture in terms of bending radius and twisting rate, the dependencies of total pump absorption at the end of the fiber are revealed in the next section.

4. Results and Discussion

Figs. 10 and 11 summarize how the pump absorption at the end of a DC fiber is dependent on the bending radius and twisting rate. The geometries G-1 and G-2 are not included in this analysis

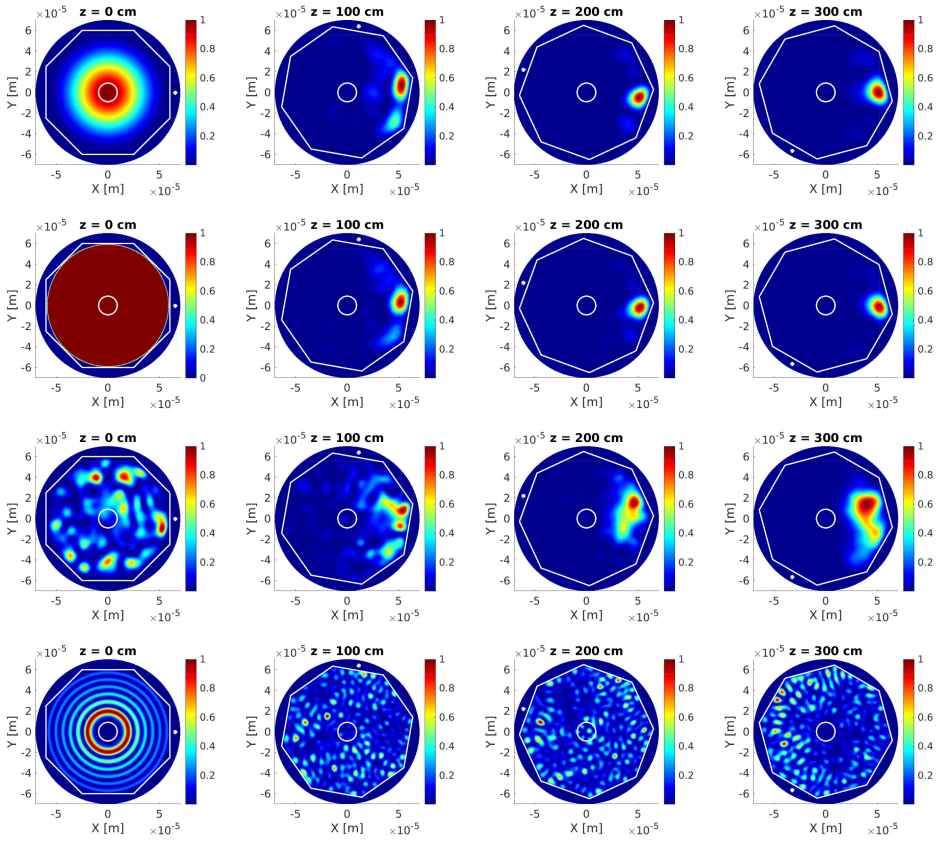

Fig. 9. Field distribution, geometry G-5 (120/18), excitation 1-4 (rows from top), bending radius $R = 4$ cm, $tr = 1$ deg/mm.

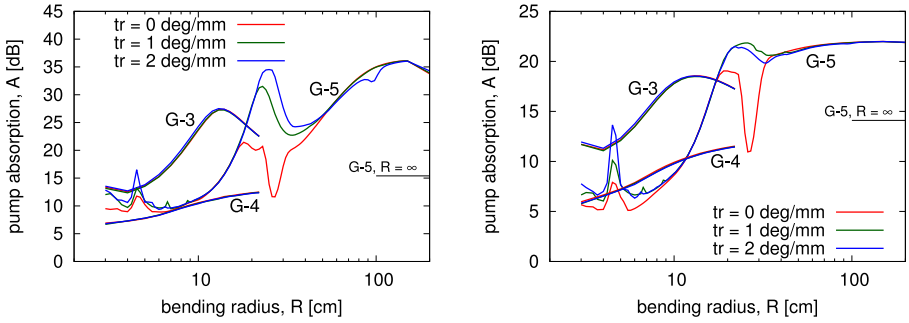

Fig. 10. Pump absorption dependence for geometries G-3 (65/14), G-4 (65/5) and G-5 (120/18). Left: excitation 1 (fundamental mode of PD fiber), right: excitation 2 (flat-top pattern). Straight fiber absorption level is denoted by $R = \infty$.

since no significant dependence on the bending radius and twisting rate was observed for these cases with the smallest cladding size. On the other hand, geometries with larger cladding size clearly exhibit an absorption sensitive to fiber perturbations.

The pump absorption in fibers with geometries G-3 and G-4 (FtF $= 65$ μm) are generally not much sensitive to twisting rate. In the case of fundamental mode and flat-top field excitation, the absorption increases with bending radius but in the geometry G-3 (65/14) it reaches its maximum at

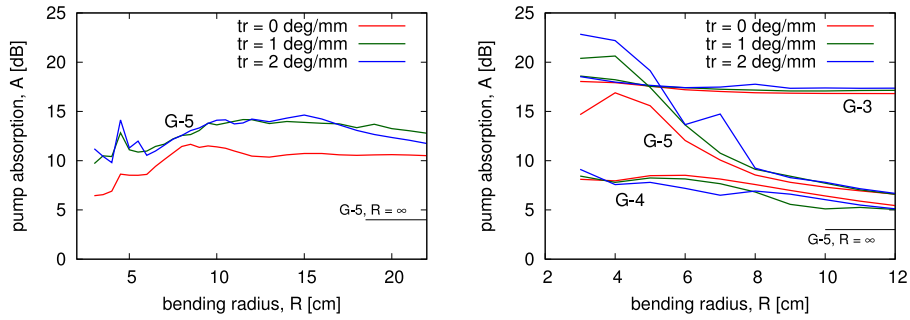

Fig. 11. Pump absorption dependence for geometries G-3 (65/14), G-4 (65/5) and G-5 (120/18). Left: excitation 3 (speckle pattern), right: excitation 4 (EH_{54} mode for geometries G-3, G-4 and EH_{76} mode for geometry G-5). Straight fiber absorption level is denoted by $R = \infty$.

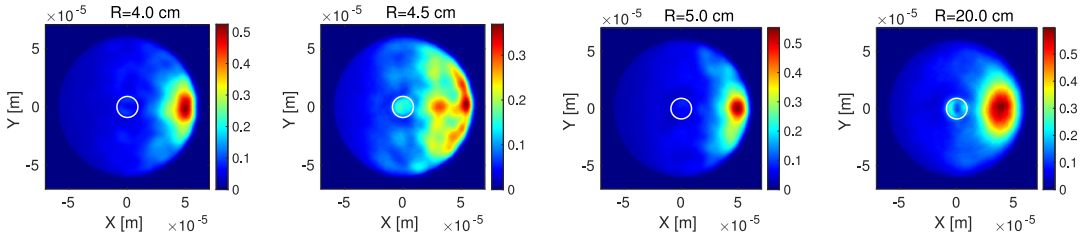

Fig. 12. Average field along the fiber, geometry G-5 (120/18), $tr = 2$ deg/mm, excitation 2 (flat-top).

around $R = 13$ cm and then decreases to its asymptotic value below 15 dB. Since the $A_{\text{ideal}} = 30$ dB at the end of 3 m long fiber, the simulated absolute values of absorption should be be compared with this value. It is seen that the higher material absorption of the core in geometry G-4 (65/5) is not enough to compensate the smaller area of the core and the resulting pump absorption does not approach A_{ideal} in any case of excitation.

The pertinent results of geometry G-5 (120/18) are the following. In cases of excitation by a fundamental mode, a flat-top field and a speckle field, the pump absorption for $R < 15$ cm is generally increasing with the bending radius. However the local maximum of absorption is observed at around $R = 4.5$ cm in all 3 cases. The region was studied in more detail with smaller steps in bending radius and results obtained seem to be consistent with presence of such local extremum. Furthermore, absorption increases with the twisting rate in that region. The peak in absorption at around $R = 4.5$ cm is attributed to the particular combination of perturbation parameters leading to a larger probability of field being localized in the central region of the fiber cross-section including a doped core. This can be seen when the average field is evaluated by means of averaging of a normalized field along the fiber. The average field P_{av} is calculated as

$$P_{\text{av}}(x, y) = \frac{1}{N} \sum_{i=1}^{N} P_z(x, y, z_i) \tag{6}$$

where $P_z(x, y, z_i)$ is the *normalized* z-component of the Poynting vector that is determined in the cross-section slice with a longitudinal coordinate z_i. Fig. 12 shows the average field for different bending radii R and flat-top excitation. The field was averaged over longitudinal distances $z_i = (0{:}1{:}50)$ cm. The average field in the core is clearly nonzero in cases $R = 4.5$ cm and 20 cm but almost vanishes in cases $R = 4$ cm and 5 cm. For fundamental mode and flat-top excitation fields, the pump absorption reaches further maxima at around $R = 25$ cm and 150 cm. Then it decreases steadily down to the $A \approx 15$ dB that is an asymptotic value for very large bending radii.

TABLE 3
Octagon Double Cladding Fiber Simulations Results

Geometry	Excitation	Relation to A_{ideal}	Effect of R	Effect of tr
G-1 (30/10)	fundamental	$A_{1\mathrm{m}} > A_{\mathrm{ideal}}$	✗	✗
	flat-top	$A_{1\mathrm{m}} > A_{\mathrm{ideal}}$	✗	✗
	skew-ray	$A_{1\mathrm{m}} \ll A_{\mathrm{ideal}}$	✓	✗
G-2 (30/5)	fundamental	$A_{1\mathrm{m}} > A_{\mathrm{ideal}}$	✓	✗
	flat-top	$A_{1\mathrm{m}} \approx A_{\mathrm{ideal}}$	✗	✗
	skew-ray	$A_{1\mathrm{m}} \ll A_{\mathrm{ideal}}$	✗	✗
G-3 (65/14)	fundamental	$A_{1\mathrm{m}} \approx A_{\mathrm{ideal}}$	✓✓	✗
	flat-top	$A_{1\mathrm{m}} \approx A_{\mathrm{ideal}}$	✓✓	✗
	skew-ray	$A_{1\mathrm{m}} \approx A_{\mathrm{ideal}}$	✓	✗
G-4 (65/5)	fundamental	$A_{1\mathrm{m}} < A_{\mathrm{ideal}}$	✓✓	✗
	flat-top	$A_{1\mathrm{m}} < A_{\mathrm{ideal}}$	✓✓	✗
	skew-ray	$A_{1\mathrm{m}} < A_{\mathrm{ideal}}$	✓	✓
G-5 (120/18)	fundamental	$A_{1\mathrm{m}} \approx A_{\mathrm{ideal}}$	✓✓✓	✓✓
	flat-top	$A_{1\mathrm{m}} \approx A_{\mathrm{ideal}}$	✓✓✓	✓✓
	speckle	$A_{1\mathrm{m}} \approx A_{\mathrm{ideal}}$	✓✓✓	✓✓
	skew-ray	$A_{1\mathrm{m}} \approx A_{\mathrm{ideal}}$	✓✓✓	✓✓✓

The effect of perturbation parameters on pump absorption is evaluated as follows: ✗ ...no effect, ✓✓✓ ...the most significant effect.

The twisting increases absorption of the speckle pattern field in the whole region of bending radii considered as shown in Fig. 11. In the case of skew-ray mode excitation, twisting increases absorption mainly for radii lower than 6 cm where the pump absorption reaches its maximal values but the effect of twisting diminishes with increasing R. The different character of the absorption dependence on the bending radius for excitations 1-4 shown in Figs. 10 and 11 indicates that the skew-ray modes are affected by bending in a qualitatively different way than the meridional-ray modes.

For the better understanding of the impact of the initial excitation fields and the longitudinal perturbation such as bending radius and twisting rate, an overview is provided in Table 3 of the observed effects of R and tr on the pump absorption in different scenarios considered in this study. In the table, $A_{1\,\mathrm{m}}$ denotes pump absorption at 1 m distance that is compared to A_{ideal}.

5. Conclusion

The presented results demonstrate that the pump absorption in the DC fiber with octagonal shape of inner cladding is significantly dependent on the particular combination of geometrical parameters of a DC fiber, the parameters of longitudinal perturbation (bending radius and twisting rate) and also on the spatial distribution of the excitation field.

Numerical simulations of five geometrical scenarios with cross-sections of a different flat-to-flat size and core radius suggest that longitudinal perturbations considered have not a big impact on pump absorption in a DC fiber with the smallest area of inner cladding with FtF of 30 μm regardless of the core radius. The number of propagating modes supported by the smallest structure is quite small and mode structure is relatively stable. The fiber bending and twisting in the amount analyzed here is not sufficient to change the mode structure notably. The absorption in medium sized geometries with FtF of 65 μm is more sensitive to fiber bending but not much to fiber twisting. Finally the absorption in the largest cross-section structure with FtF of 120 μm exhibits the largest sensitivity to both bending and twisting and is also notably dependent on the excitation field.

To conclude, the current work motivated by the applications of tandem pumped holmium doped high power fiber lasers provides further insight into the subject that has been widely studied but

not completely understood so far; namely the question how the pump absorption in DC fibers relates to parameters of longitudinal perturbations. To our knowledge, this study revealed for the first time the detailed dependencies of pump absorption on the bending radius and twisting rate as presented in Figs. 10 and 11 for different types of initial excitation fields. The aforementioned results substantiate that the impact of such perturbations increases with the cross-section area. While this means the effect is not too much pronounced in DC fibers with relatively small cross-sections, one can anticipate that the effect becomes more important in DC fibers with the larger cross-sections of the inner cladding, namely in the large-diameter DC fibers that are pumped directly by laser diodes.

Acknowledgment

Authors acknowledge the collaboration with CESNET e-Infrastructure. Computational resources were supplied by the project "e-Infrastruktura CZ" (e-INFRA LM2018140) provided within the program Projects of Large Research, Development and Innovations Infrastructures.

References

[1] M. N. Zervas and C. A. Codemard, "High power fiber lasers: A. review," *IEEE J. Sel. Topics Quantum Electron.*, vol. 20, no. 5, pp. 219–241, Sep. 2014.
[2] V. Khitrov, J. D. Minelly, R. Tumminelli, V. Petit, and E. S. Pooler, "3 kW single-mode direct diode-pumped fiber laser," in *Fiber Lasers XI: Technol., Syst., Appl.*, S. Ramachandran, Ed., vol. 8961, Int. Soc. Opt. Photon. SPIE, 2014, pp. 137–142.
[3] S. Liu *et al.*, "Yb-doped aluminophosphosilicate triple-clad laser fiber with high efficiency and excellent laser stability," *IEEE Photon. J.*, vol. 11, no. 2, Apr. 2019, Art. no. 1501010.
[4] S. K. Kalyoncu, B. Mete, and A. Yeniay, "Diode-pumped triple-clad fiber MOPA with an output power scaling up to 4.67 kW," *Opt. Lett.*, vol. 45, no. 7, pp. 1870–1873, Apr. 2020.
[5] "10.6 kW high-brightness cascade-end-pumped monolithic fiber lasers directly pumped by laser diodes in step-index large mode area double cladding fiber," *Results Phys.*, vol. 14, 2019, Art. no. 102479.
[6] H. Zhan *et al.*, "Pump-gain integrated functional laser fiber towards 10 kW-level high-power applications," *Laser Phys. Lett.*, vol. 15, no. 9, Jul. 2018, Art. no. 095107.
[7] B. Shiner, "The impact of fiber laser technology on the world wide material processing market," in *Proc. CLEO: Appl. Technol.*, 2013, p. AF2J.1.
[8] V. P. Gapontsev, "25 years of the high power fiber lasers," presented at the OSA Laser Congr.: Adv. Solid State Lasers (ASSL) Laser Appl. Conf., Boston, MA, USA, 2020.
[9] P. Zhou *et al.*, "High-power fiber lasers based on tandem pumping," *J. Opt. Soc. B*, vol. 34, no. 3, pp. A 29–A36, Mar. 2017.
[10] A. Hemming, N. Simakov, J. Haub, and A. Carter, "A review of recent progress in holmium-doped silica fibre sources," *Opt. Fiber Technol.*, vol. 20, no. 6, pp. 621–630, 2014.
[11] M. Kamrádek *et al.*, "Nanoparticle and solution doping for efficient holmium fiber lasers," *IEEE Photon. J.*, vol. 11, no. 5, Oct. 2019, Art. no. 7103610.
[12] S. D. Jackson, "Towards high-power mid-infrared emission from a fibre laser," *Nat. Photon.*, vol. 6, no. 7, pp. 423–431, 2012.
[13] L. G. Holmen *et al.*, "Tunable holmium-doped fiber laser with multiwatt operation from 2025 nm to 2200 nm," *Opt. Lett.*, vol. 44, no. 17, pp. 4131–4134, Sep. 2019.
[14] A. Hemming, S. Bennetts, N. Simakov, A. Davidson, J. Haub, and A. Carter, "High power operation of cladding pumped holmium-doped silica fibre lasers," *Opt. Exp.*, vol. 21, no. 4, pp. 4560–4566, Feb. 2013.
[15] C. C. Baker *et al.*, "Recent advances in holmium doped fibers for high-energy lasers," in *Proc. Laser Technol. Defense Secur. XIV*, M. Dubinskiy and T. C. Newell, Eds., vol. 10637, Int. Soc. Opt. Photon. SPIE, 2018, Art. no. 1063704.
[16] A. A. Jasim, O. Podrazký, P. Peterka, M. Kamrádek, I. Kašík, and P. Honzátko, "Impact of shaping optical fiber preforms based on grinding and a CO_2 laser on the inner-cladding losses of shaped double-clad fibers," *Opt. Exp.*, vol. 28, no. 9, pp. 13601–13615, Apr. 2020.
[17] P. C. Shardlow *et al.*, "Holmium doped fibre optimised for resonant cladding pumping," in *Proc. Eur. Conf. Lasers Electro-Optics Eur. Quantum Electron. Conf.*, 2017, Paper CJ_ 11_4.
[18] A. A. Jasim *et al.*, "Efficient pump absorption in twisted double clad thulium-doped fibers drawn of CO_2 laser shaped preform," in *Proc. Eur. Conf. Lasers Electro-Optics*, 2019, Paper cj_p_ 8.
[19] J. Nilsson, S. U. Alam, J. A. Alvarez-Chavez, P. W. Turner, W. A. Clarkson, and A. B. Grudinin, "High-power and tunable operation of erbium-ytterbium co-doped cladding-pumped fiber lasers," *IEEE J. Quantum Electron.*, vol. 39, no. 8, pp. 987–994, Aug. 2003.
[20] L. Shang and Z. Song, "Characteristics of pump mode distribution in a double-clad fiber with octagonal inner cladding," *Optoelectron. Adv. Mat.*, vol. 4, no. 5, pp. 613–615, 2010.
[21] H. Zellmer, A. Tünnermann, H. Welling, and V. Reichel, "Double-clad fiber laser with 30 W output power," in *Optical Amplifiers and Their Applications* (ser. OSA Trends in Optics and Photonics Series), Jul. 21, 1997.
[22] M. Xu, J. Cao, Z. Huang, and S. Guo, "Study of fiber coiling methods and pump light absorption," *Guangxue Xuebao/Acta Opt. Sinica*, vol. 34, pp. s106008–s106011, Sep. 2014.

[23] C. A. Codemard, A. Malinowski, and M. N. Zervas, "Numerical optimisation of pump absorption in doped double-clad fiber with transverse and longitudinal perturbation," in *Proc. Fiber Lasers XIV: Technol. Syst., Ser. Proc. SPIE*, C. A. Robin and I. Hartl, Eds., International Society for Optics and Photonics. SPIE, vol. 10083, 2017, pp. 208–214.
[24] P. Peterka *et al.*, "Optimization of erbium-ytterbium fibre laser with simple double-clad structure," in *Photon., Devices, Syst. III*, P. Tománek, M. Hrabovský, M. Miler, and D. Senderákova, Eds., vol. 6180, International Society for Optics and Photonics. SPIE, 2006, pp. 213–218.
[25] F. Todorov *et al.*, "Active optical fibers and components for fiber lasers emitting in the 2-μm spectral range," *Materials*, vol. 13, no. 22, 2020, Art. no. 5177.
[26] P. Koška, P. Peterka, I. Kašík, V. Matějec, and O. Podrazký, "Double-clad rare-earth-doped fiber with cross-section tailored for splicing to the pump and signal fibers: Analysis of pump propagation," in *Micro-structured Specialty Optical Fibres II*, K. Kalli, J. Kanka, and A. Mendez, Eds., Int. Soc. Opt. Photon. SPIE, vol. 8775, 2013, pp. 190–195.
[27] P. Koška and P. Peterka, "Numerical analysis of pump propagation and absorption in specially tailored double-clad rare-earth doped fiber," *Opt. Quantum Electron.*, vol. 47, no. 9, pp. 3181–3191, 2015.
[28] P. Koška, P. Peterka, and V. Doya, "Numerical modeling of pump absorption in coiled and twisted double-clad fibers," *IEEE J. Sel. Topics Quantum Electron.*, vol. 22, no. 2, pp. 55–62, Mar. 2016.
[29] P. Koška *et al.*, "Enhanced pump absorption efficiency in coiled and twisted double-clad thulium-doped fibers," *Opt. Exp.*, vol. 24, no. 1, pp. 102–107, 2016.
[30] R. Dalidet, P. Peterka, V. Doya, J. Aubrecht, and P. Koška, "Pump absorption in coiled and twisted double-clad hexagonal fiber: Effect of launching conditions and core location," in *SPIE Photonics West: Fiber Lasers XV, Ser. Proc. SPIE*, vol. 10512, 2018, Art. no. 105122.
[31] M. Grábner, K. Nithyanandan, P. Peterka, P. Koška, P. Honzátko, and A. A. Jasim, "Numerical modelling of pump absorption in coiled and twisted double-clad fiber: A prospect for tandem pumped fiber laser," in *Micro-Structured Specialty Opt. Fibres VI*, K. Kalli, P. Peterka, and C.-A. Bunge, Eds., Int. Soc. Opt. Photon. SPIE, vol. 11355, 2020, pp. 133–138.
[32] J. Wang *et al.*, "Numerical modeling of in-band pumped Ho-doped silica fiber lasers," *J. Lightw. Technol.*, vol. 36, no. 24, pp. 5863–5880, Dec. 2018.
[33] C. Geuzaine and J.-F. Remacle, "Gmsh: A 3-D finite element mesh generator with built-in pre- and post-processing facilities," *Int. J. Num. Meth. Eng.*, vol. 79, pp. 1309–1331, Sep. 2009.
[34] M. Heiblum and J. Harris, "Analysis of curved optical waveguides by conformal transformation," *IEEE J. Quantum Electron.*, vol. 11, no. 2, pp. 75–83, Feb. 1975.